Polarization instabilities of dark and bright coupled solitary waves in birefringent optical fibers

S. Wabnitz
Fondazione Ugo Bordoni, Via Baldassare Castiglione 59, 00142 Rome, Italy

E. M. Wright and G. I. Stegeman
Optical Sciences Center, University of Arizona, Tucson, Arizona 85721
(Received 18 December 1989)

We investigate the stability of the propagation of bright and dark coupled solitary waves that may travel in the orthogonal polarization modes of a birefringent nonlinear optical fiber. In the anomalous dispersion regime, the coupled-solitary-wave decay is self-induced by modulational polarization instability of the dark component background pulse. In the normal dispersion regime, stable propagation only occurs for distances of the order of one linear beat length. We identify different instability mechanisms such as gray soliton formation, polarization wave breaking, polarization dispersion, and self-stimulated Raman scattering that leads to asymmetric coupled-solitary-wave breakup.

I. INTRODUCTION

There is a growing interest in studying the propagation of optical soliton pulses in fibers, in view of their potential application to fiber-optic-based communication systems, lasers, and switching devices. Since ultrashort soliton pulses are stable against dispersive spreading, they are attractive for ultrahigh bit-rate long-distance time-division multiplexed optical communication systems. The validity of this early proposal[1] has recently been confirmed by experimental evidence.[2] On the other hand, the propagation of soliton pulses enjoys other important properties such as self-compression and particlelike behavior: this has been successfully exploited for ultrashort pulse shaping in lasers[3] and for all-optical switching.[4,5]

As is well known, nonlinear pulse propagation in a single-mode fiber is described by the nonlinear Schrödinger (NLS) equation, which, in the anomalous group-velocity dispersion (GVD) regime, has soliton solutions propagating as *bright* pulses.[6] In the normal dispersion regime (that is, for wavelengths below 1.3 μm in nondispersion-shifted fibers), NLS solitons occur in the form of dips embedded in a continuous background,[7] and have been termed *dark* or *gray* solitons.[8-11]

Henceforth, propagation of temporally localized or bright solitary pulses in the visible may not occur in optical fibers, unless some coupling between two distinct guided modes is exploited. In fact, it is known from plasma theory that the coupling with a transverse electromagnetic wave may lead to the localization of a Langmuir wave packet for otherwise forbidden wavelengths.[12] Coupled solitary waves may also arise from the coupled NLS equations describing the interaction between Langmuir and ion-acoustic waves or between two transverse polarized electromagnetic waves in a plasma[13] or in a magneto-optically active medium.[14] In the context of nonlinear fiber optics, it was first pointed out in Ref. 15 that cross-phase modulation (CPM) between any two copropagating fiber modes could sustain optical coupled solitary waves. In particular, a bright solitary wave may propagate in the normal dispersion regime, when coupled with a dark pulse in the anomalous dispersion regime. Note that this interaction requires a careful tuning of wavelengths in order to insure group-velocity matching between the two pulses.

From a practical standpoint, it would be desirable to avoid coupled solitary pulses with distinct mean wavelengths. In fact, as was proposed in Ref. 16, dark and bright coupled solitary waves may also result, both in the normal and in the anomalous dispersion regime, from the interaction between the two orthogonal polarization modes of a birefringent fiber.

In the above cases, dispersive temporal broadening of a short pulse that propagates in the normal dispersion regime is compensated by nonlinear coupling. We may mention here that an alternative approach to propagating bright solitons at visible wavelengths is modifying the dispersive properties of the fiber itself through linear mode coupling.[17] In fact, recent analyses have shown that bright soliton propagation in fiber filters may occur, both in the copropagating[18] and in the counterpropagating[19-21] (or distributed feedback) geometry.

A solitary-wave solution of a nonlinear wave equation is properly termed soliton if it represents a physically *stable* wave packet. This is always the case if the problem is completely integrable by means of the inverse scattering transform: Then each soliton is characterized by a discrete set of eigenvalues in the complex scattering plane. Unfortunately, the coupled NLS equations describing propagation in two-mode fibers are *not* completely integrable (except for very special cases[22-24]); therefore, the stability issue is of primary importance for their solitary-wave solutions.

The stability of coupled-solitary-wave solutions of the CPM-coupled NLS equations has been studied by variational, perturbative, and numerical methods by several authors.[14,25-27] When linear coupling occurs between the modes, as in the case of circularly polarized waves in a birefringent fiber,[28] a relatively complex picture of soliton instabilities emerges from the stability analysis.[29] In

this work we concentrate on the interesting case of coupled bright and dark solitary pulses propagating in a birefringent fiber.[16] These solitary-wave solutions exist both in the normal and in the anomalous GVD regime, but we shall see that the stability properties are rather different in the two cases. The various instabilities will be revealed by beam propagation simulations and the physical mechanisms behind them will be identified. In particular, the model shall include temporal walkoff due to polarization dispersion, and stimulated Raman scattering (SRS).

II. DARK-BRIGHT COUPLED SOLITARY WAVES

The transverse electric field $\mathbf{E}(\mathbf{r},z,t)$ traveling along a weakly guiding single-mode birefringent fiber is decomposed in terms of orthogonal linearly polarized modes:

$$\begin{aligned}\mathbf{E}(\mathbf{r},z,t)&=[\mathbf{x}f_x(\mathbf{r})A_x(z,t)+\mathbf{y}f_y(\mathbf{r})A_y(z,t)]e^{-i\omega_0 t}+\text{c.c.}\\&=[\mathbf{x}f_x(\mathbf{r})\mathcal{A}_x(z,t)e^{i\beta_x z}\\&\quad+\mathbf{y}f_y(\mathbf{r})\mathcal{A}_y(z,t)e^{i\beta_y z}]e^{-i\omega_0 t}+\text{c.c.}\ ,\end{aligned}$$

where ω_0 is the mean optical frequency, $f_x(\mathbf{r})\cong f_y(\mathbf{r})$ are the transverse field distributions of the linearly polarized modes, and $\mathbf{x},\mathbf{y}$ are unit vectors oriented as the birefringence axes, with linear propagation constants $\beta_{x,y}=\omega_0 n_{x,y}/c$. In glass fibers the electronic (nonresonant) third-order nonlinear polarizability is completely symmetric and reads[30]

$$\mathbf{P}^{(3)}_{\mathrm{NR}i}(\mathbf{r},z,t)=\sigma_{ijkl}E_j(t)E_k(t)E_l(t)\ ,$$

where $i,j,k,l=x,y$ and

$$\sigma_{ijkl}=\chi(\delta_{ij}\delta_{kl}+\delta_{ik}\delta_{jl}+\delta_{il}\delta_{jk})\ .$$

Here δ_{ij} is the Kronecker δ. Hence the complex field amplitudes $A_{x,y}$ obey the coupled NLS equations[31]

$$\begin{aligned}&i\frac{\partial A_x}{\partial z}+i\frac{1}{V_x}\frac{\partial A_x}{\partial t}-\frac{\alpha}{2}\frac{\partial^2 A_x}{\partial t^2}+\beta_x A_x\\&\qquad+R(|A_x|^2+\tfrac{2}{3}|A_y|^2)A_x+(R/3)A_x^* A_y^2=0\ ,\end{aligned}\tag{1}$$

$$\begin{aligned}&i\frac{\partial A_y}{\partial z}+i\frac{1}{V_y}\frac{\partial A_y}{\partial t}-\frac{\alpha}{2}\frac{\partial^2 A_y}{\partial t^2}+\beta_y A_y\\&\qquad+R(|A_y|^2+\tfrac{2}{3}|A_x|^2)A_y+(R/3)A_y^* A_x^2=0\ .\end{aligned}$$

Here $V_{x,y}=(\partial\beta_{x,y}/\partial\omega)^{-1}|_{\omega_0}$ are the modal group velocities, whereas $\alpha\cong\partial^2\beta_{x,y}/\partial^2\omega|_{\omega_0}$ is the chromatic dispersion, which can be assumed to be common to both polarizations. Finally, the nonlinearity coefficient $R(W^{-1}m^{-1})=\omega_0 n_2/cA_{\mathrm{eff}}$, where $n_2(m^2/W)$ is the nonlinear refractive index and A_{eff} is the effective core area. By writing Eqs. (1) in a time-retarded frame and in terms of dimensionless units, one obtains

$$\begin{aligned}&i\frac{\partial u}{\partial\zeta}+i\delta\frac{\partial u}{\partial s}\pm\tfrac{1}{2}\frac{\partial^2 u}{\partial s^2}+\kappa u+(|u|^2+\tfrac{2}{3}|v|^2)u+\tfrac{1}{3}u^* v^2=0\ ,\\&i\frac{\partial v}{\partial\zeta}-i\delta\frac{\partial v}{\partial s}\pm\tfrac{1}{2}\frac{\partial^2 v}{\partial s^2}-\kappa v+(|v|^2+\tfrac{2}{3}|u|^2)v+\tfrac{1}{3}v^* u^2=0\ ,\end{aligned}\tag{2}$$

where the plus and minus signs hold in the case of anomalous or normal dispersion, respectively. We have used the following normalized coordinates and field amplitudes:

$$\begin{aligned}&s\equiv(t-z/V)/t_s,\quad \zeta\equiv z/z_c=|\alpha|z/t_s^2\ ,\\&u\equiv(Rt_s^2/|\alpha|)^{1/2}A_x e^{-i\beta z}\ ,\\&v\equiv(Rt_s^2/|\alpha|)^{1/2}A_y e^{-i\beta z}\ ,\end{aligned}$$

where $2\beta=\beta_x+\beta_y$ and t_s is the temporal width of the fundamental bright NLS soliton,[1] which would propagate for on-axis input polarization [i.e., $v(\zeta=0,s)=0$ or $u(\zeta=0,s)=0$ in Eqs. (2)]. Furthermore, $V\equiv 2V_xV_y/(V_x+V_y)\cong(V_x+V_y)/2$, $\delta=(n_x-n_y)t_s/2|\alpha|c$, and $\kappa=(n_x-n_y)\omega_0 t_s^2/2|\alpha|c=\delta\omega_0 t_s$.

By neglecting the contribution of the polarization dispersion δ (we shall discuss the effect of δ in a later section of the paper), one obtains the following solitary-wave solution of Eqs. (2):[16]

$$\begin{aligned}&u=U_0\,\mathrm{sech}(s/s_0)e^{i(\sigma-\kappa)\zeta}\ ,\\&v=V_0\tanh(s/s_0)e^{i(\sigma+\kappa)\zeta}\ ,\end{aligned}\tag{3}$$

where one must take $\kappa>0$ in the case of normal dispersion and $\kappa<0$ for anomalous GVD. In other words, the bright solitary wave travels along the slow (fast) axis of the fiber whenever the dispersion is normal (anomalous). The amplitudes and width are

$$U_0^2=(\rho-3\kappa),\quad V_0^2=(\rho+\kappa),\quad s_0^2=\frac{1}{4\kappa}\ .\tag{4}$$

The quantity ρ is an arbitrary positive constant. Equation (4) shows that the temporal width of the pulses (3) equals the NLS soliton width t_s for $\kappa=\frac{1}{4}$. In the following sections we shall present numerical investigations of the stability of the solutions (3) and (4) of Eqs. (2). In fact, the nonlinear coupling between the modal amplitudes u and v is strong, which prevents the applicability of a perturbative stability analysis as was done in Ref. 27 for weakly interacting dark-bright coupled solitary waves.

III. MODULATIONAL POLARIZATION INSTABILITY

We have integrated Eqs. (2) by a modified version of the beam propagation or split-step method with up to 2048 temporal grid points. In the calculations, the birefringence term is included in the dispersive step, whereas the nonlinear step may be carried out immediately if Eqs. (2) are transformed in the corresponding equations for the components of the circular polarization basis.[28] We assumed initial conditions as given by Eqs. (3), with a finite-width Gaussian background pulse superimposed to the dark solitary wave,

$$u(\zeta=0,s)=U_0\mathrm{sech}(s/s_0)\ ,$$
$$v(\zeta=0,s)=V_0\tanh(s/s_0)e^{-s^2/2\sigma^2}\ . \tag{5}$$

Consider first the anomalous dispersion regime: Then we must set $\kappa<0$ in Eqs. (2), which means that the dark pulse v is the slow mode component. Figure 1 shows the evolution of intensities in the two linear polarizations, when $U_0^2=3$ and $V_0^2=2$, whereas the coupled-solitary-wave width $s_0=1$. The variance of the background pulse is $\sigma=12.5$. As can be seen, the dark pulse component is unstable: modulational instability[32] (MI) is self-induced at the edges of the dip and leads to breakup of the slow axis component into a train of high-intensity pulses with a repetition period approximately equal to $2s_0$ (see Fig. 2, which shows the intensity in the slow mode for $\zeta=5$). Note that there is characteristic distance for the development of MI: the coupled solitary wave propagates virtually unchanged for a distance $\zeta\cong3$. Subsequently, dark pulse breakup is followed by substantial polarization conversion from the fast to the slow mode. The bright pulse in the fast mode does not decay into radiation but rather remains localized with a complex temporal structure. Note that in the absence of polarization coupling, the hyperbolic secant pulse with peak power $U_0^2=3$ would evolve into a longitudinally periodic $N=2$ NLS soliton.

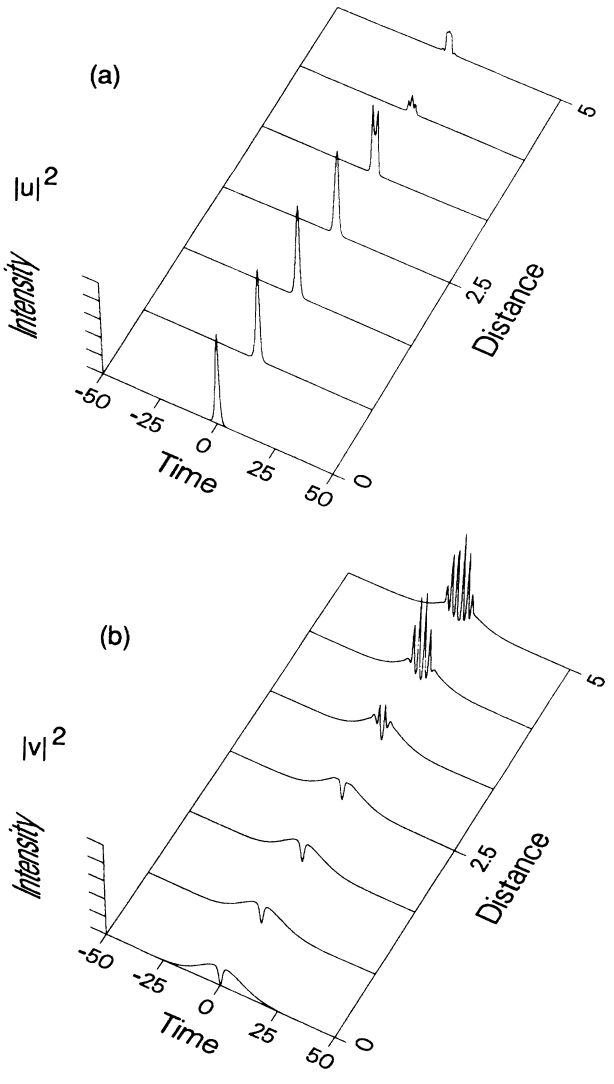

FIG. 1. Propagation in the anomalous dispersion regime. Evolution of intensities of (a) the bright solitary-wave component u (fast mode), and (b) the dark solitary wave v (slow mode). Intensities are in arbitrary units: The values have been normalized both in (a) and (b) to the peak values. Time and distance are in the soliton units of Eq. (2).

The condition $s_0=1$ implies $|\kappa|=\pi\delta n t_s^2/(|\alpha|\lambda)=\frac{1}{4}$, or $L_b=4\pi t_s^2/|\alpha|$, where $\delta n=|n_x-n_y|$ and $L_b=\delta n/\lambda$ is the beat length. Therefore, with a dispersion $\alpha=-0.018$ ps^2/m at $\lambda=1.5$ μm, one obtains a soliton width $t_{\mathrm{FWHM}}=1.76t_s=70$ fs with $L_b=1$ m. Note that the peak power of the bright pulse $U_0^2=3$ is well above the threshold power for continuous wave (cw) modulational instability[33] (or polarization instability[34,35]), which is equal to $U^2=p_c\equiv3\kappa=\frac{3}{4}$. This instability leads to the growth of sidebands in the slow mode, which explains the polarization conversion that is seen in Fig. 1. In physical units, assuming an effective area $A_{\mathrm{eff}}=6.5\times10^{-7}$ cm^2, and with $n_2=3.2\times10^{-16}$ cm^2/W, one obtains a bright pulse peak power $P_u=8\lambda A_{\mathrm{eff}}/n_2L_b=24$ kW.

IV. FINITE BACKGROUND EFFECTS

From now on, we shall only consider coupled-solitary-wave propagation in the normal dispersion regime. In this section and in Sec. V we shall discuss the effects of varying the background pulse width σ relative to the soliton temporal width s_0.

Whenever $\alpha>0$, if one takes $\kappa>0$, then u (v) is the slow (fast) mode component. Figure 3 shows the evolution of intensities in the two polarizations with initial conditions (5), $U_0^2=2$, $V_0^2=3$, $s_0=1$, and a background pulse variance $\sigma=7.5$. As can be seen, due to dispersive temporal broadening of the background, after $\zeta\cong3$ the dark pulse decays and so does the bright one. After a transitory region where the peak intensity of the

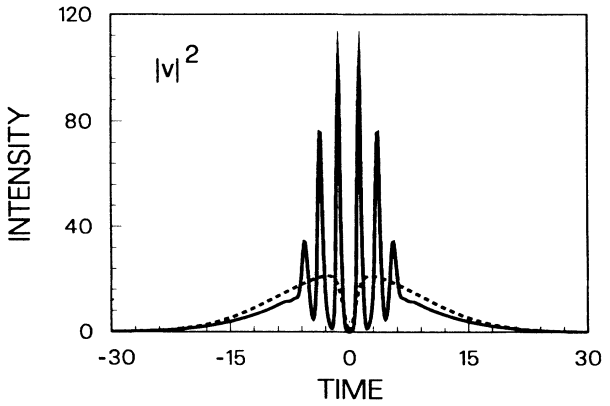

FIG. 2. Intensities of input dark pulse (dashed curve) and of propagated pulse at a distance $\zeta=5$, as in Fig. 1(b). The intensity scale is given in arbitrary units, time is in soliton units.

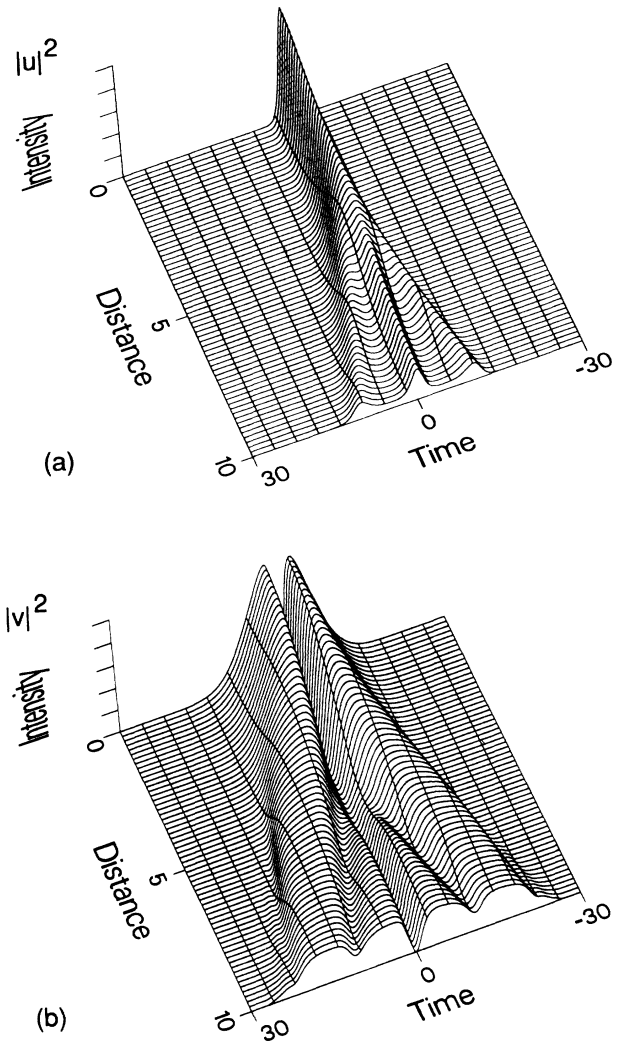

FIG. 3. Propagation in the normal dispersion regime: (a) evolution of bright solitary wave u (slow-mode component) and (b) intensity of dark pulse v (fast mode). Bright-dark pulse widths are equal to the fundamental soliton width, i.e., $s_0=1$. Dark soliton background pulse width $\sigma=7.5$. Time and distance are in soliton units.

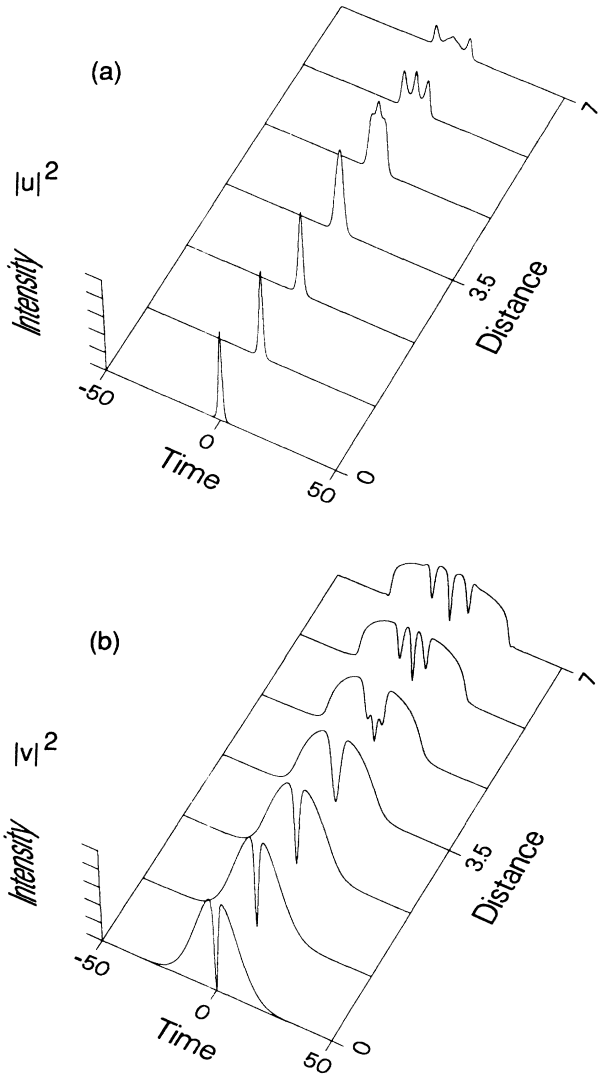

FIG. 4. As in Fig. 3, with a background pulse width $\sigma=12.5$.

coupled-solitary-wave components decreases, a new periodic temporal structure appears. A low-intensity dark-bright coupled solitary wave forms at the center of the pulse, while two gray-bright coupled solitary waves move away from it with, respectively, lower and higher relative group velocities. Note that a similar evolution into dark-gray solitons also occurs for isolated finite-background dark pulses in the single-mode propagation case.[36]

As shown in Figs. 4–7, this situation persists whenever the background pulse width grows larger. Figure 4 shows the intensities of the coupled-solitary-wave components, with input conditions given as in Fig. 3, and $\sigma=12.5$. The distance where the coupled solitary wave decays is not appreciably different from the previous case, and so is for the velocity of the gray pulses relative to the dark one. Figure 5 illustrates initial and final intensity profiles as in Fig. 4 for a distance $\zeta=7$: While the central dip remains a proper odd-symmetry dark soliton whose time width is unchanged with respect to the initial one, its bright counterpart gets substantially broadened. As one would expect, the dark soliton component of the pair is substantially more stable than its bright counterpart.

Figure 6 displays coupled-solitary-wave evolutions with $\sigma=30$: Here a slight increase of the distance where the pair decays results. As shown by Fig. 7, which portrays the input and output (for $\zeta=7$) pulses in the fast mode, the contrast ratio and the relative velocity of the gray and dark pulses remain essentially unchanged with respect to the previous cases.

In physical units, we may take, for example, $\lambda=600$ nm, where the fused silica dispersion is $D=350$ psec/nm km, or $\alpha=\lambda^2 D/2\pi c\cong 0.068$ ps^2/m: With $L_b=1$ m, the condition $s_0=1$ corresponds to a temporal width $t_{\mathrm{FWHM}}=130$ fs for the coupled-solitary wave, whereas $L_b=25$ cm would yield a 65-fs width. With an

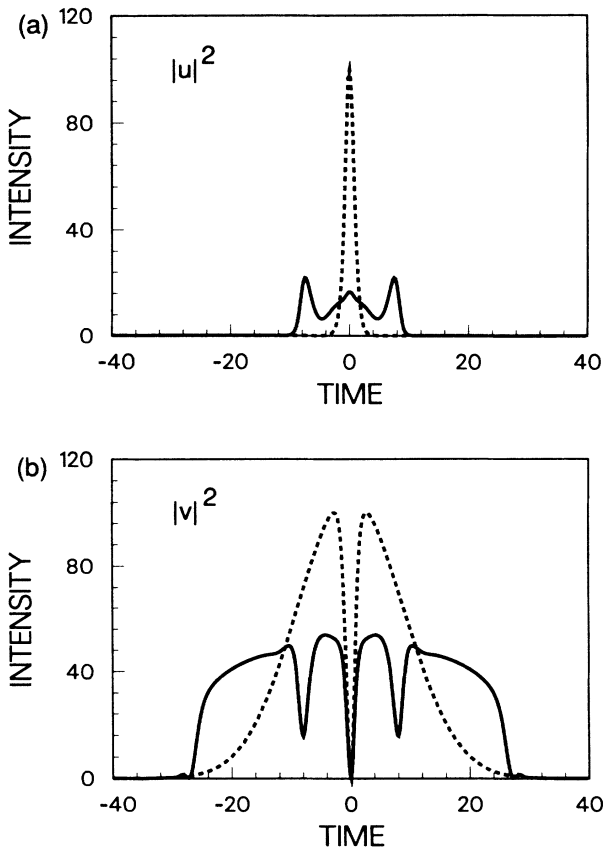

FIG. 5. Intensities of (a) input (dashed curve) and propagated bright pulse for $\zeta=7$; (b) same as in (a), for the dark pulse, with a width $\sigma=12.5$.

effective area $A_{\text{eff}}=1\times10^{-7}$ cm^2, the peak power of the bright component would be $P_u=1.5$ or 6 kW, respectively. Finally, the normalized distance $\zeta=1$ corresponds to $z_c=L_b/4\pi\cong8$ cm with $L_b=1$ m.

V. POLARIZATION WAVE BREAKING

Until now we have only considered the case $s_0=1$: In this section we shall present results of simulations where the coupled-solitary-wave width (with respect to the NLS soliton width t_s) is varied. In particular, we shall elucidate that the freedom in choosing the coupled-solitary-wave time width s_0 in Eqs. (4) is only formal. In fact, whenever the wavelength and the fiber birefringence are fixed, different choices for s_0 only imply a rescaling of coordinates but all of them will correspond to the same actual pulse time width.

Figure 8 illustrates the evolution of the polarization components for initial conditions as in Eqs. (5) with $s_0=\frac{1}{2}$ (i.e., $\kappa=1$), $U_0^2=8$, and $V_0^2=12$. The background pulse width is $\sigma=30$ as in the previous figure. As can be seen, gray soliton formation is closely followed by breakup of the coupled-solitary-wave polarization components into a rapidly varying irregular wave train. The dark component appearing at the propagation distance $\zeta=10$ is shown in Fig. 9, along with the input pulse profile.

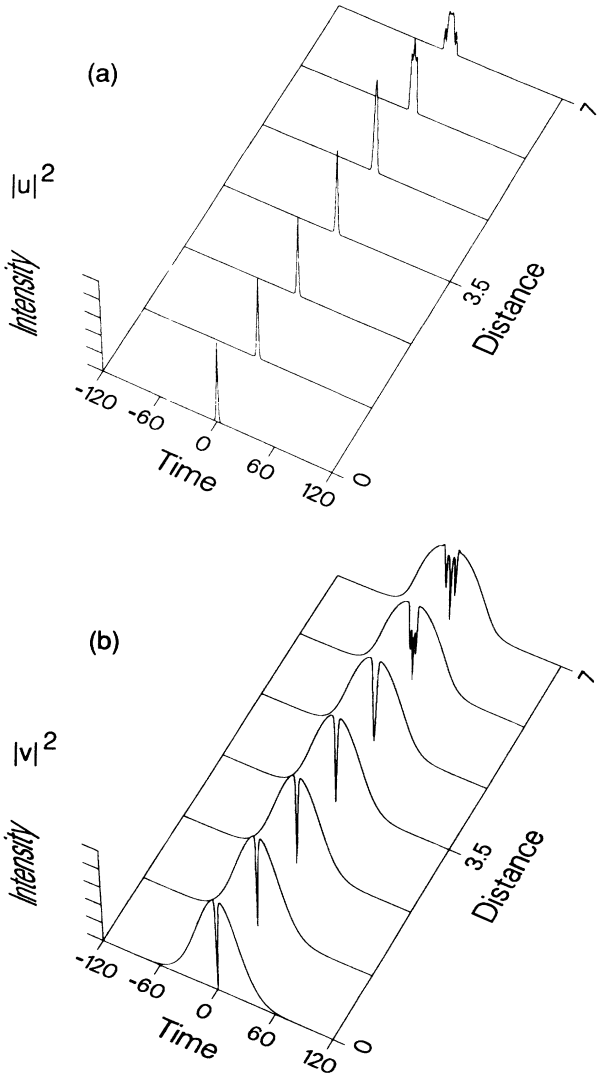

FIG. 6. As in Fig. 3, with a background pulse width $\sigma=30$.

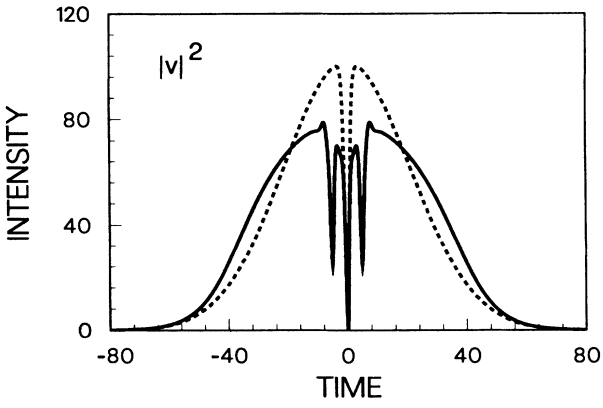

FIG. 7. Intensities of input (dashed curve) and propagated dark pulses for a distance $\zeta=7$, with a width $\sigma=30$.

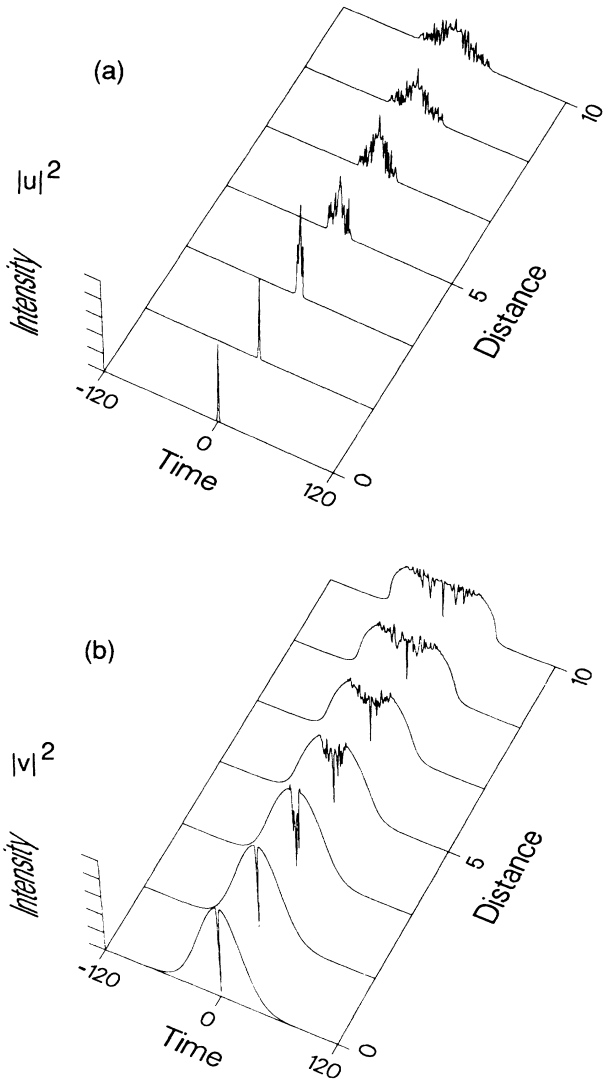

FIG. 8. As in Fig. 3, when the coupled dark-bright soliton width is half the width of the fundamental NLS soliton (i.e., $s_0=\frac{1}{2}$).

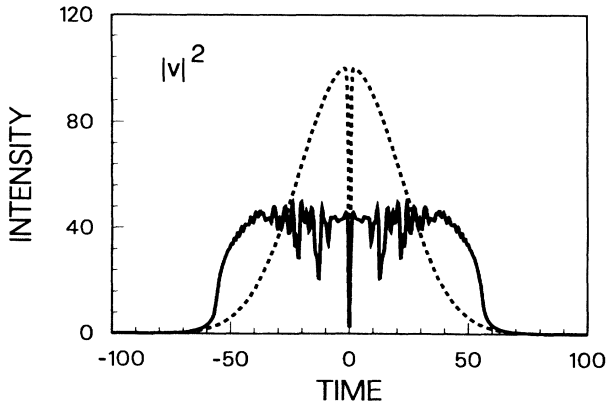

FIG. 9. Intensities of input (dashed curve) and propagated dark pulse after a distance $\zeta=10$, as in Fig. 8(b).

Again, a substantial amount of energy is converted with distance from the fast mode (v) to the slow mode. The origin of this instability is therefore the modulational instability that may occur in a birefringent fiber also in the normal dispersion regime.[33] In fact, when the fast axis is pumped by a quasicontinuous wave of peak power $p_v > p_c = 3\kappa$, orthogonally polarized weak sidebands with angular frequency detunings up to the cutoff frequency[33]

$$\Omega_c = 2[(p_v/p_c - 1)\kappa]^{1/2} \tag{6}$$

would experience exponential growth along the propagation distance. Here MI of the dark pulse is induced by the presence of the orthogonally polarized spectral components of the bright pulse. Note that this instability did

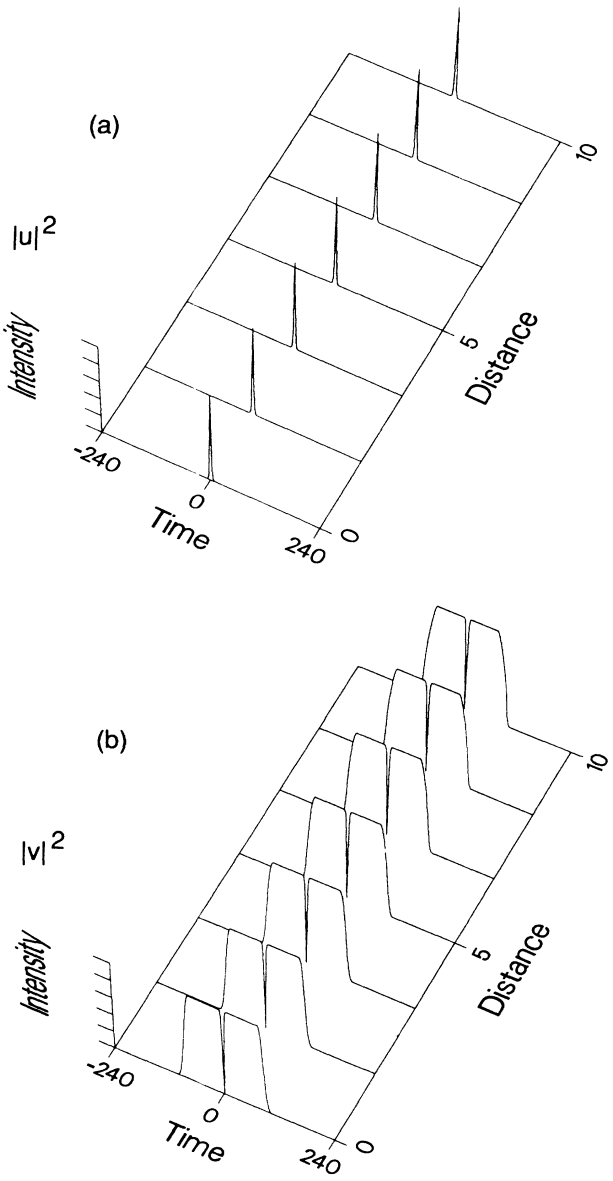

FIG. 10. Same as in Fig. 3, with a square background for the dark pulse. In this case, the coupled-solitary-wave width is twice the fundamental soliton width (i.e., $s_0=2$). Background square pulse width is $\sigma_{\mathrm{FWHM}}=160$.

not appear up to $\zeta=10$ in the previous simulations with $s_0=1$ since the pulse intensities were four times lower and this correspondingly reduced the instability gain per unit of normalized distance.

On the other hand, Fig. 10 shows that stable coupled-solitary-wave propagation results, as least for $\zeta<10$, whenever $s_0=2$ ($\kappa=\frac{1}{16}$). In this case, we took $U_0^2=\frac{1}{2}$, $V_0^2=\frac{3}{4}$, and a square background pulse with a temporal width of 160 temporal units. From the expression for the normalized parameter κ, one sees that, for a given value of the beat length, κ can be reduced four times by halving the time t_s. Since this also increases by a factor of 4 the peak powers, this means that the actual coupled-solitary-wave time width and peak powers corresponding to Figs. 3–9 and 10, with L_b fixed, are the same. In other words, the arbitrariness in choosing the coupled-solitary-wave time width s_0 that results from Eqs. (4) is fictitious. In fact, in order to get the same physical distance as in Figs. 3–7, the normalized distance in Fig. 10 should be increased by a factor of 4, which explains the propagation stability in Fig. 10.

VI. POLARIZATION DISPERSION

In all of the previous simulations we have neglected the presence of group-velocity walkoff between the two orthogonal polarizations, or polarization dispersion δ. Since $\delta=\kappa\lambda/(2\pi t_s c)$, polarization dispersion cannot possibly be discarded when providing a realistic estimate of the maximum distance over which the coupled-solitary-wave solution maintains its stable identity during propagation. If this has been done up to now, this was justified by the interest in gaining a separate understanding of effects leading to the various types of instability.

Figures 11 and 12 were obtained by assuming $\lambda=615$ nm, $D=350$ ps/nm km, $L_b=1$ m, which yields $\delta=1.1\times10^{-3}$. This corresponds to a group delay difference between the linear polarization modes of only 2 ps/km. The initial conditions are the same as in Fig. 3, that is, $\kappa=\frac{1}{4}$, $U_0^2=2$, and $V_0^2=3$, whereas the background square pulse width is equal to 60 time units. As can be seen, the dark pulse travels on the fast mode and arrives at the distance $\zeta=10$ slightly in advance with respect to the center of the background (see Fig. 12), while the gray satellite pulses are asymmetrically distorted. At the same time, the bright component is completely broken up into a rapidly oscillating wave train as soon as $\zeta>7$. This indicates that even a small polarization dispersion may set a practical limit to the validity of the coupled-solitary-wave solution [(3) and (4)] to about half of the birefringence beat length.

VII. SELF-STIMULATED RAMAN SCATTERING

As we have seen, for typical birefringence beat lengths (that is, of 1 m or less) the temporal width of the coupled solitary wave is of the order of 100 fs. For such short pulses, the noninstantaneous contribution to the nonlinear response of the fiber or self-stimulated Raman scattering may be important.[30] In fact, Raman scattering may be self-activated by the mixing, through the Raman

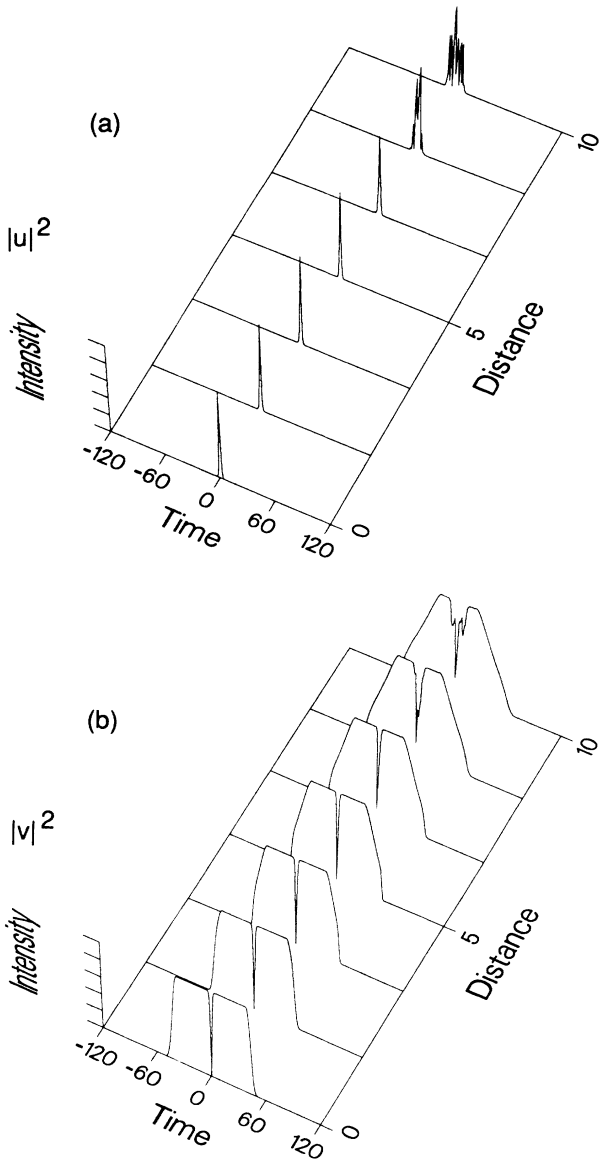

FIG. 11. Breakup due to polarization dispersion. The initial conditions are as in Fig. 3.

susceptibility, among the lower and higher frequency components of a pulse. In the anomalous dispersion regime, this effect leads to a continuous downshift of the mean frequency of a soliton.[37] Nonlinear pulse propagation in optical fibers in the presence of Raman scattering may be described in the time domain by adding a delayed nonlinear term to the NLS equation.[38–40] We extend here previous scalar treatments to the case of two coupled polarizations [Eqs. (1)]. We may write the total third-order polarizability as $\mathbf{P}^{(3)}=\mathbf{P}^{(3)}_{\rm NR}+\mathbf{P}^{(3)}_{\rm R}$. The resonant part can be written, in the Born-Oppenheimer approximation,[30] as a convolution integral

$$\mathbf{P}^{(3)}_{{\rm R}i}(t)=E_j(t)\int_{-\infty}^{+\infty} ds\, f_{ijkl}(t-s)E_k(s)E_l(s)\ , \qquad (7)$$

where the tensorial Raman response function $f_{ijkl}(t)$ reads

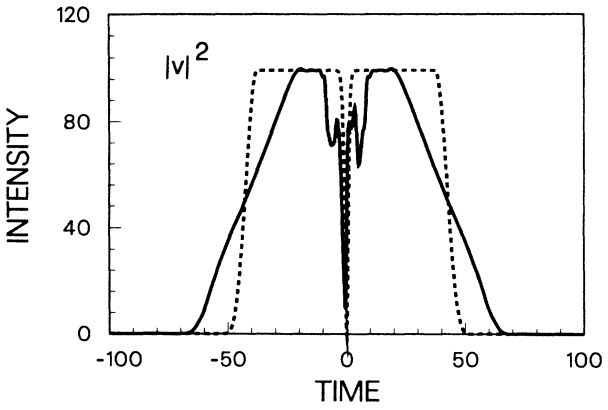

FIG. 12. Intensities of input pulse (dashed curve) and of propagated pulse (solid curve) for a propagation distance $\zeta=10$, as in Fig. 11(b).

$$f_{ijkl}(t)=a(t)\delta_{ij}\delta_{kl}+\tfrac{1}{2}b(t)(\delta_{il}\delta_{jk}+\delta_{ik}\delta_{jl}) ,$$
$$i,j,k,l=x,y . \quad (8)$$

Clearly when a single polarization mode is involved, one recovers the familiar Raman causal response function $g(t)=f_{iiii}(t)=a(t)+b(t)$. By inserting the expression (8)

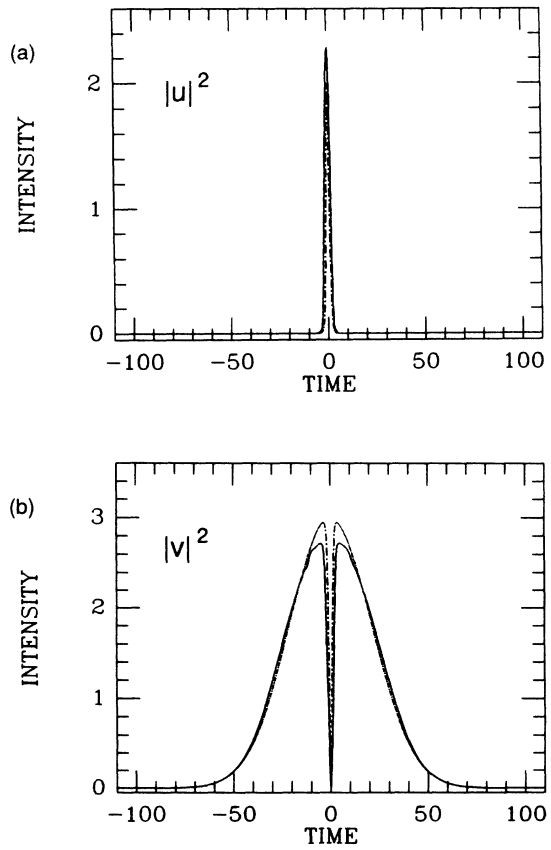

FIG. 13. Effect of self-stimulated Raman scattering: (a) the input (dashed curve) and propagated (solid curve) bright pulses at a distance $\zeta=5$ are shown and (b) the same for the dark pulse component.

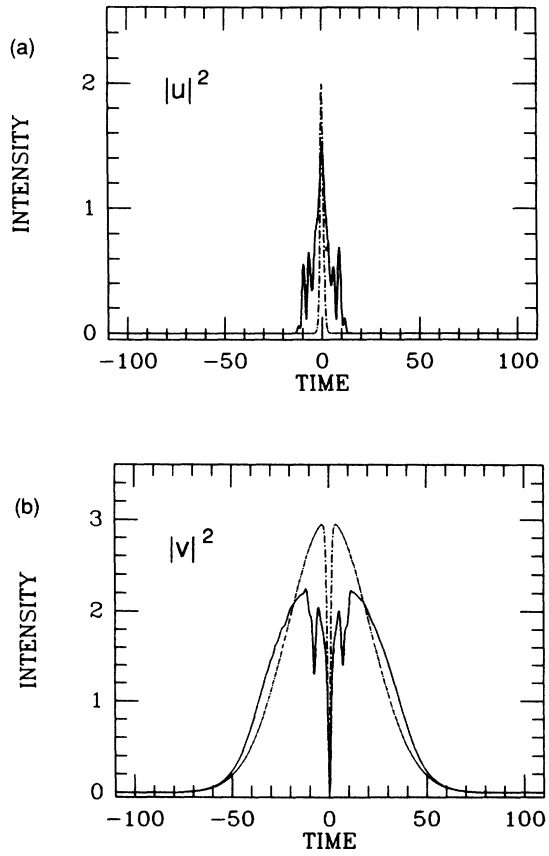

FIG. 14. Same as in Fig. 13, for a propagation distance $\zeta=10$.

into Eq. (7), one obtains for the normalized complex field envelopes u and v the modified coupled NLS equations

$$i\frac{\partial u}{\partial\zeta}+i\delta\frac{\partial u}{\partial s}\pm\tfrac{1}{2}\frac{\partial^2 u}{\partial s^2}+\kappa u+\eta(|u|^2+\tfrac{2}{3}|v|^2)u+\frac{\eta}{3}u^*v^2$$
$$+(1-\eta)\int_{-\infty}^{s}d\tau g(s-\tau)[|u(\tau)|^2+|v(\tau)|^2]=0 , \quad (9)$$

$$i\frac{\partial v}{\partial\zeta}-i\delta\frac{\partial v}{\partial s}\pm\tfrac{1}{2}\frac{\partial^2 v}{\partial s^2}-\kappa v+\eta(|v|^2+\tfrac{2}{3}|u|^2)v+\frac{\eta}{3}v^*u^2$$
$$+(1-\eta)\int_{-\infty}^{s}d\tau g(s-\tau)[|u(\tau)|^2+|v(\tau)|^2]=0 .$$

Here $\eta\cong 0.8$,[38] and we have neglected the contribution of $b(t)$ with respect to $a(t)$.[30] This approximation may be justified by the fact that in silica the depolarized Raman cross section [which is the Fourier transform of $b(t)$] is more than one order of magnitude smaller than the parallel one. The fused quartz Raman response function $g(t)$ can be well approximated by[40]

$$g(t)=\frac{\tau_1^2+\tau_2^2}{\tau_1\tau_2^2}\exp(-t/\tau_2)\sin(t/\tau_1) , \quad (10)$$

with $\tau_1=12.2$ fs and $\tau_2=33$ fs.

Figures 13 and 14 show results of the propagation of bright and dark pulse components in the normal dispersion regime, when computed by integrating Eqs. (9) and

(10) for distances $\zeta=5$ and 10, respectively. The initial conditions were given as in Figs. 6 and 7: $U_0^2=2$, $V_0^2=3$, $s_0=1$, and $\sigma=30$. We also assumed a coupled-solitary-wave width $t_{\mathrm{FWHM}}=130$ fs at the wavelength $\lambda=600$ nm. As can be seen, up to $\zeta=5$ the effect of self-SRS is negligible, and the bright pulse is even slightly amplified at the expense of the dark one, whereas for distances as large as $\zeta=10$, the bright and the dark pulses acquire a slight asymmetry while breaking up. As occurs for single-mode NLS dark solitons,[41] the gray solitons have now different depths, which appear, however, much reduced when compared with the gray pulse depths (obtained with purely instantaneous response) that are shown in Fig. 7.

Qualitatively similar results are obtained with different choices for the expressions approximating the Raman response function (for example, a simple exponential decay), or with different choices for the symmetry of the delayed tensorial nonlinearity. In order to present an extreme case, we may consider a purely relaxing tensorial third-order susceptibility,

$$i\frac{\partial u}{\partial \zeta}+i\delta\frac{\partial u}{\partial s}\pm\tfrac{1}{2}\frac{\partial^2 u}{\partial s^2}+\kappa u+\chi u+\phi v=0\ ,$$
$$i\frac{\partial v}{\partial \zeta}-i\delta\frac{\partial v}{\partial s}\pm\tfrac{1}{2}\frac{\partial^2 v}{\partial s^2}-\kappa v+\eta u+\phi^* v=0\ , \tag{11}$$
$$\tau\frac{\partial \chi}{\partial s}+\chi=|u|^2+\tfrac{1}{3}|v|^2\ ,$$
$$\tau\frac{\partial \eta}{\partial s}+\eta=|v|^2+\tfrac{1}{3}|u|^2\ , \tag{12}$$
$$\tau\frac{\partial \phi}{\partial s}+\phi=\tfrac{1}{3}uv^*+\text{c.c.}$$

In the limit $\tau\Longrightarrow 0$, the above equations reduce to Eqs. (2). Equations of this type may describe, for example, the effect of stimulated Rayleigh-Kerr scattering on the propagation of ultrashort pulses in carbon disulphide (CS_2) liquid-core fibers,[42] where linear birefringence can be induced by applying a static electric field.

Figures 15 and 16 show bright and dark coupled-solitary-wave propagation when solving Eqs. (11) and (12) with the same input conditions as in Figs. 13 and 14. The relaxation time was assumed $\tau=0.1t_s$. As can be seen, the bright and dark pulses become strongly asymmetric

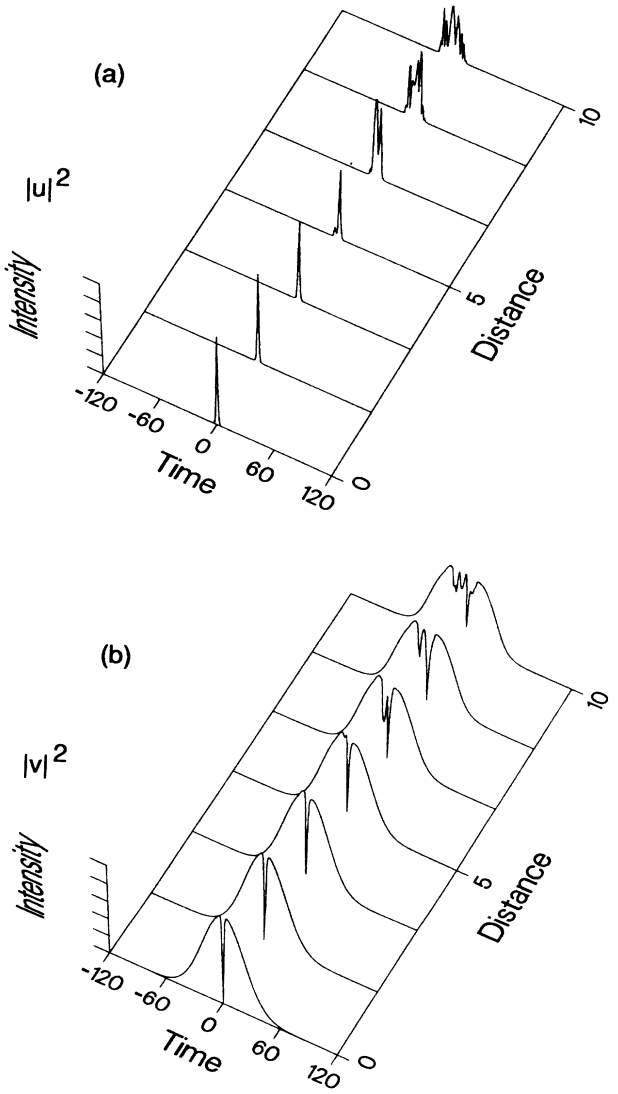

FIG. 15. Same as in Fig. 6, with a purely relaxing third-order susceptibility.

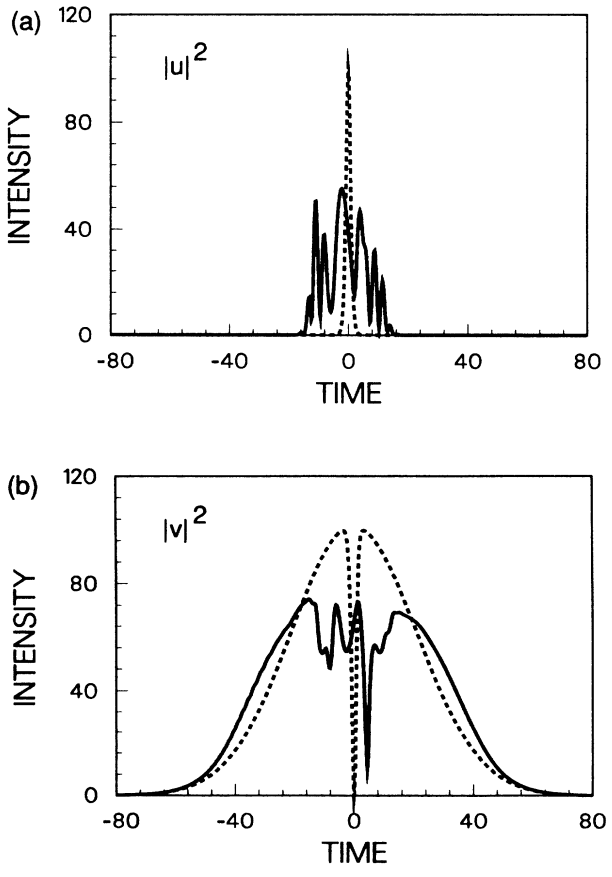

FIG. 16. Coupled-solitary-wave components as in Fig. 15 at the fiber input (dashed lines) and after a propagation distance $\zeta=10$ (solid lines).

as soon as $\zeta > 5$: In particular, the dark pulse shifts in time, which prevents the formation of the slower gray soliton until $\zeta \cong 10$. Furthermore, the distortion and wave breaking of the bright component appears to be more dramatic here than in the previous case [compare Figs. 14(b) and 16(b)].

VIII. CONCLUSIONS

We investigated the propagation stability of coupled dark and bright solitons in birefringent fibers, both in the normal and in the anomalous dispersion regime. We have individuated different physical mechanisms that may concur in breaking up the coupled solitary wave, such as modulational and polarization instabilities, polarization dispersion, and self-stimulated Raman scattering. The analysis has shown that stable propagation only occurs over a limited distance, which typically is of the order of one linear beat length of the fiber.

ACKNOWLEDGMENTS

We thank D. N. Christodoulides and K. J. Blow for kindly sending copies of their papers prior to publication. This work was supported by the U.S. Air Force Office of Scientific Research (Grant No. 87-0344). The work of one of us (S.W.) was supported by the U.S. Army Research Office Grant No. DAAL01-88-K-0066 during his visit at the Optical Sciences Center where this work was carried out, and by Fondazione Ugo Bordoni in the framework of the agreement with the Istituto Superiore Poste e Telecomunicazioni. CPU time from the John von Neumann Computer Center is gratefully acknowledged.

[1]A. Hasegawa and F. Tappert, Appl. Phys. Lett. **23**, 142 (1973).
[2]L. F. Mollenauer and K. Smith, Opt. Lett. **13**, 675 (1988).
[3]L. F. Mollenauer and R. H. Stolen, Opt. Lett. **9**, 13 (1984); K. Suzuki, M. Nakazawa, and H. Haus, *ibid.* **14**, 320 (1989).
[4]K. J. Blow, N. J. Doran, and B. K. Nayar, in *Technical Digest of the Topical Meeting on Nonlinear Guided-Wave Phenomena* (Optical Society of America, Washington, D.C., 1989), paper PD7; K. J. Blow, N. J. Doran, and B. K. Nayar, Opt. Lett. **14**, 754 (1989).
[5]M. N. Islam, E. R. Sunderman, R. H. Stolen, W. Pleibel, and J. R. Simpson, in *Technical Digest of the Topical Meeting on Nonlinear Guided-Wave Phenomena,* (Optical Society of America, Washington, D.C., 1989), paper PD8; M. N. Islam, E. R. Sunderman, R. H. Stolen, W. Pleibel, and J. R. Simpson, Opt. Lett. **14**, 754 (1989).
[6]V. E. Zakharov and A. B. Shabat, Zh. Eksp. Teor. Fiz. **61**, 118 (1971) [Sov. Phys.—JETP **34**, 62 (1972)].
[7]V. E. Zakharov and A. B. Shabat, Zh. Eksp. Teor. Fiz. **64**, 1627 (1973) [Sov. Phys.—JETP **37**, 823 (1973)].
[8]A. Hasegawa and F. Tappert, Appl. Phys. Lett. **23**, 171 (1973).
[9]P. Emplit, J. P. Hamaide, F. Reynaud, C. Froehly, and A. Barthelemy, Opt. Commun. **62**, 374 (1987).
[10]D. Krokel, N. J. Halas, G. Giuliani, and D. Grischkowsky, Phys. Rev. Lett. **60**, 29 (1988).
[11]A. M. Weiner, J. P. Heritage, R. J. Hawkins, R. N. Thurston, E. M. Kirschner, D. E. Leaird, and W. J. Tomlinson, Phys. Rev. Lett. **61**, 2445 (1988).
[12]M. R. Gupta, B. K. Som, and B. Dasgupta, J. Plasma Phys. **25**, 499 (1981).
[13]K. P. Das and S. Sihi, J. Plasma Phys. **21**, 183 (1979).
[14]V. K. Mezentsev and G. I. Smirnov, Opt. Commun. **68**, 153 (1988).
[15]S. Trillo, S.. Wabnitz, E. M. Wright, and G. I. Stegeman, Digest of the Fourteenth European Conference on Optical Communication, Brighton, U.K., 1988 (unpublished), pp. 107; Opt. Lett. **13**, 871 (1988).
[16]D. N. Christodoulides, Phys. Lett. **132**, 451 (1988).
[17]H. G. Winful, Appl. Phys. Lett. **46**, 527 (1985).
[18]S. Wabnitz, Opt. Lett. **14**, 1071 (1989).
[19]D. N. Christodoulides and R. I. Joseph, Phys. Rev. Lett. **62**, 1746 (1989).
[20]C. M. de Sterke and J. E. Sipe, Opt. Lett. **14**, 871 (1989).
[21]A. B. Aceves and S. Wabnitz, Phys. Lett. A **141**, 37 (1989).
[22]S. V. Manakov, Zh. Eksp. Teor. Fiz. **65**, 505 (1973).
[23]V. E. Zakharov and E. I. Schulman, Physica D **4**, 270 (1982).
[24]R. Sahadevan, K. M. Tamizhmani, and M. Lakshmanan, J. Phys. A **19**, 1783 (1986).
[25]J. C. Bhakta and M. R. Gupta, J. Plasma Phys. **28**, 379 (1982).
[26]V. V. Afanasyev, E. M. Dianov, A. M. Porkhorov, and V. N. Serkin, Pis'ma Zh. Eksp. Teor. Fiz. **48**, 588 (1988).
[27]V. V. Afanasyev, Yu. S. Kivshar, V. V. Konotop, and V. N. Serkin, Opt. Lett. **14**, 805 (1989).
[28]K. J. Blow, N. J. Doran, and D. Wood, Opt. Lett. **12**, 202 (1987).
[29]E. M. Wright, G. I. Stegeman, and S. Wabnitz, Phys. Rev. A **40**, 4455 (1989).
[30]R. W. Hellwarth, Prog. Quantum Electron. **5**, 1 (1977).
[31]B. Crosignani and P. Di Porto, Opt. Acta **32**, 1251 (1985).
[32]K. Tai, A. Hasegawa, and A. Tomita, Phys. Rev. Lett. **56**, 135 (1986).
[33]S. Wabnitz, Phys. Rev. A **38**, 2018 (1988); S. Trillo, and S. Wabnitz, J. Opt. Soc. Am. B **6**, 238 (1989).
[34]B. Daino, G. Gregori, and S. Wabnitz, J. Appl. Phys. **58**, 4512 (1985); Opt. Lett. **11**, 42 (1986).
[35]H. G. Winful, Opt. Lett. **11**, 33 (1986).
[36]W. J. Tomlinson, R. J. Hawkins, A. M. Weiner, J. P. Heritage, and R. N. Thurston, Opt. Soc. Am. B **6**, 329 (1989).
[37]J. P. Gordon, Opt. Lett. **11**, 662 (1986).
[38]R. H. Stolen, J. P. Gordon, W. J. Tomlinson, and H. A. Haus, J. Opt. Soc. Am. B **6**, 1159 (1989).
[39]E. A. Golovchenko, E. M. Dianov, A. Ya. Karasik, P. V. Mamyshev, A. N. Pilipetskii, and A. M. Prokhorov, Kvant. Electron. (Moscow) **16**, 592 (1989).
[40]K. J. Blow and D. Wood, IEEE J. Quantum Electron. **QE-25**, 2665 (1989).
[41]A. M. Weiner, R. N. Thurston, W. J. Tomlinson, J. P. Heritage, D. E. Leaird, E. M. Kirschner, and R. J. Hawkins, Opt. Lett. **14**, 868 (1989).
[42]G. S. He and P. N. Prasad, Opt. Commun. **73**, 161 (1989).